PURIFICATION OF RUTILE IN SRI LANKAN BEACH SAND FOR THE EXTRACTION OF TiO_2 BY REDUCING IRON CONTENT

Weerasinge Damith Chathuranga Weerasinghe

(198117L)

Degree of Master of Science

Department of Materials Science and Engineering

University of Moratuwa
Sri Lanka

August 2024

PURIFICATION OF RUTILE IN SRI LANKAN BEACH SAND FOR THE EXTRACTION OF TiO_2 BY REDUCING IRON CONTENT

Weerasinge Damith Chathuranga Weerasinghe

(198117L)

Thesis submitted in partial fulfillment of the requirements for the degree Master of Science in Materials Science and Engineering

Department of Materials Science and Engineering

University of Moratuwa

Sri Lanka

August 2024

DECLARATION

"I declare that this is my own work and this dissertation does not incorporate without acknowledgement any material previously submitted for a Degree or Diploma in any other University or institute of higher learning and to the best of my knowledge and belief, it does not contain any material previously published or written by another person except where the acknowledgement is made in the text.

Also, we hereby grant the University of Moratuwa the non-exclusive right to reproduce and distribute our dissertation in whole or in part in print, electronic or other mediums. I retain the right to use this content in whole or part in future works (such as articles or books)."

Signature: Date: 13.08.2024

W.D.C. Weerasinghe

The above candidate has carried out research for the Master's thesis under my supervision.

Signature of the supervisor: Date: 23.08.2024

Eng. S. P. Guluwita.

Signature of the supervisor: Date: 23.08.2024

Dr. L. P. S. Rohitha.

ACKNOWLEDGMENT

I would like to pay special thankfulness, warmth and appreciation to my research supervisor, Eng. S. P. Guluwita, Department of Materials Science and Engineering not only for his guidance throughout my research but also for the knowledge and tips he has shared with me. I thank him for his encouragement that made it possible to achieve the goal and also for playing a significant role in my career development by giving me guidance and support. Next, I would like to thank Dr. L. P. S. Rohitha, Department of Earth Resources Engineering for the supervision and support throughout the project. Also my sincere gratitude to Dr. (Mrs) N. M. V. K. Liyanage and Dr. (Mrs) A. S. Galhenage from the University of Moratuwa for their immense support and academic push throughout the evaluation procedure.

I would like to thank Mr. V. Sivahar, Head of the Department of Materials Science and Engineering and all the academic and non-academic staff of the Department of Materials Science and Engineering and Department of Earth Resources Engineering for supporting us with the knowledge and laboratory facilities.

Finally, I would like to thank all the research assistants who helped to succeed of this research. I would like to give my heartiest gratitude to all of them for being with me.

Weerasinghe W.D.C

(198117L)

ABSTRACT

The Pulmuddai region in Sri Lanka is characterized by key constituents: 55-60% ilmenite, 6-8% rutile, and 5-6% iron. Iron's presence emerges as a critical impurity necessitating pre-extraction removal for titanium dioxide extraction from rutile. Attaining a TiO_2 purity exceeding 99% within rutile is attainable through targeted iron elimination and meticulous optimization of the purification process. The methodological approach commences with the initial screening and separation of beach sand, utilizing the Humphrey spiral technique to selectively isolate high-density minerals enriched with rutile and ilmenite. Subsequent separation of rutile from ilmenite employs a magnetic separator. The conclusive step involves the strategic removal of iron from rutile via leaching with hydrochloric acid (HCl). Optimization of leaching parameters, including the solid-to-liquid ratio (S/L ratio), HCl concentration, and reaction time, maximizes iron removal from rutile. A comprehensive analysis of samples before and after leaching employs a UV-visible spectrophotometer and scanning electron microscopy utilizing Energy Dispersive X-Ray Spectroscopy on the samples. Results indicate 83.3% reduction in iron content within rutile from the initial raw mineral, achieved under optimized conditions of 1:3 S/L ratio, 80°C, 4-hour reaction time, and 4M HCl concentration.

Keywords: *Titanium dioxide, Pulmuddai, Rutile, Purification.*

TABLE OF CONTENTS

DECLARATION i

ACKNOWLEDGMENT ii

ABSTRACT iii

TABLE OF CONTENTS iv

LIST OF FIGURES v

LIST OF TABLES vi

ABBREVIATIONS vii

1. INTRODUCTION 8

1.1 Introduction to Titanium 8

1.2 Introduction to Titanium Dioxide 11

1.3 Objectives 12

2. LITERATURE REVIEW 13

2.1 Titanium: Applications, Production, and Economic Implications 13

2.2 Processing Methods 14

2.3 Beach Sand Deposits 16

3. METHODOLOGY 19

3.1 Materials and Apparatus 19

3.2 Separation Process 19

3.3 Purification Process 21

3.4 Method 01: Purification Process 21

3.5 Method 02: Purification Process 23

3.6 Characterization 24

4. RESULTS AND DISCUSSION 25

5. CONCLUSIONS 44

6. RECOMMENDATIONS 45

7. REFERENCES 46

LIST OF FIGURES

Figure 1.1: Titanium metal existing minerals in beach sand 8
Figure 1.3: Producing percentage of titanium by different countries in 2021 9
Figure 1.2: Major countries which produce ilmenite and rutile (2021) 9
Figure 1-4: Pumuddai Heavy Mineral Deposit 10
Figure 1-5: Products from Titanium Dioxide 11
Figure 3-1: Separation Procedure 19
Figure 3-2: Beach Sand Separation Process 20
Figure 3-3: Process of Sieve Analysis 21
Figure 3-4: Variation of the Testing Parameters in Method 01 22
Figure 3-5: Variation of the Testing Parameters in Method 02 23
Figure 4-1: Cumulative Graph for the Sieve Analysis 25
Figure 4-2: EDX Results for Initial Mineral Sample 26
Figure 4-3: Purification process for 2M concentration sample 28
Figure 4-4: Variation with Temperature & Time (Concentration 2M)(S/L ratio 1:3) 31
Figure 4-5: Variation with Temperature & Time (Concentration 3M)(S/L ratio 1:3) 35
Figure 4-6: Variation with Temperature & Time (Concentration 4M)(S/L ratio 1:2) 39

LIST OF TABLES

Table 2-1: Properties of Minerals 13
Table 4-1: Sieve Analysis Data (Cumulative Value) 25
Table 4-2: EDX Results for Initial Sample 26
Table 4-3: Summarized EDX data for Different Ranges 27
Table 4-4: Variation with Temperature & Time (Concentration 2M & 1:2 S/L Ratio) 28
Table 4-5: Variation with Temperature & Time (Concentration 2M & 1:3 S/L Ratio) 29
Table 4-6: Variation with Temperature & Time (Concentration 2M & 1:4 S/L Ratio) 30
Table 4-7: Variation with Temperature & Time (Concentration 3M & 1:2 S/L Ratio) 32
Table 4-8: Variation with Temperature & Time (Concentration 3M & 1:3 S/L Ratio) 33
Table 4-9: Variation with Temperature & Time (Concentration 3M & 1:4 S/L Ratio) 34
Table 4-10: Variation with Temperature & Time (Concentration 4M & 1:2 S/L Ratio) 36
Table 4-11: Variation with Temperature & Time (Concentration 4M & 1:3 S/L Ratio) 37
Table 4-12: Variation with Temperature & Time (Concentration 4M & 1:4 S/L Ratio) 38
Table 4-13: Summary: Results for Method 02 42

LIST OF ABBREVIATIONS

Abbreviation	Description
TiO_2	Titanium Dioxide
TEFS	Titanium-Bearing Electric Furnace Slag
HCl	Hydrochloric acid
EDX	Energy-dispersive X-ray spectroscopy
S/L	Solid to Liquid
w/w	Weight in Weight
UV	Ultraviolet
LMS	Low-intensity Magnetic Separation

1. INTRODUCTION

1.1 Introduction to Titanium

Titanium, a metallic element, is renowned for its resistance to corrosion and high temperatures, featuring a high melting point, lightweight nature, and compatibility with the human body. It occurs naturally, often combined with other elements. In the Earth's crust, titanium holds the rank of the ninth most abundant element, constituting approximately 0.63% of its composition. Predominantly found in igneous rocks and sediment, titanium is widely distributed in minerals like anatase, brookite, ilmenite, perovskite, rutile, and titanite, and is commonly present in iron ores. Beach sand contains ilmenite, rutile, monazite, zircon, sillimanite and quartz as shown in Figure 1.1. This prevalence in various natural forms positions titanium as a valuable element with diverse applications, from industrial uses to its compatibility in medical contexts due to its unique combination of properties. Understanding its abundance and distribution in nature provides valuable insights for harnessing its versatile characteristics in a range of practical applications. [1]

Figure 1.1: Titanium metal existing minerals in beach sand

Rutile, classified as a mineral, comprises around 85% titanium dioxide (TiO_2). This mineral is highly regarded for its cutting-edge attributes, notably its exceptional strength-to-weight ratio and resilience against corrosion in demanding environments. Titanium, derived from rutile, plays a pivotal role across diverse fields. Its applications span the creation of nuclear-waste canisters, castings for pacemakers, medical implants, high-performance automotive components, and armor for ordnance.

Ilmenite and rutile are produced by major countries as shown in Figure 1.2. Remarkably, approximately 5% of the global production of titanium minerals is dedicated to the production of titanium metal by various countries in 2021 as shown in Figure 1.3. This metal, with its unique properties, finds extensive use in the aircraft industry and serves various industrial applications. The utilization of rutile as a precursor to titanium metal underscores its significance as a key raw material in the production of advanced materials that contribute to technological advancements and innovation across multiple sectors. [3]

Figure 1.2: Major countries which produce ilmenite and rutile in 2021

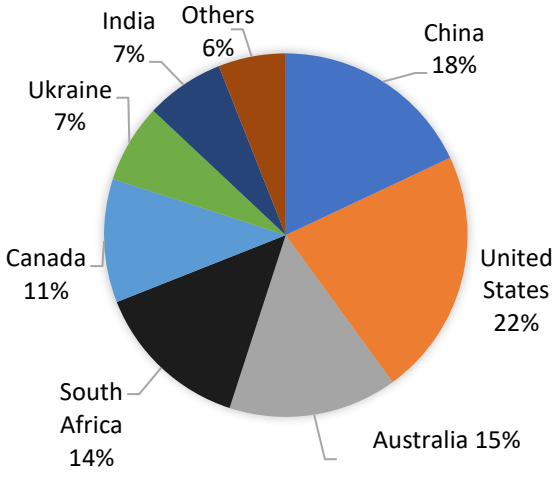

Figure 1.3: Producing percentage of titanium by different countries in 2021

Sri Lanka boasts a wealth of industrial minerals, such as graphite, ilmenite, rutile, zircon, quartz, feldspar, clay, kaolin, apatite (Phosphate rock), silica Sand, garnet sand, mica, calcite, and dolomite. Notably, the Pulmuddai beach sand deposit stands out as the country's most significant non-ferrous mineral reserve as shown in Figure 1.4. This deposit, rich in various minerals including titanium, is acknowledged as one of the world's most valued and sought-after metals. The Pulmuddai deposit underscores Sri Lanka's prominence in the global mineral landscape, particularly in the realm of non-ferrous resources. Understanding and harnessing these abundant mineral resources hold considerable importance for both domestic industrial development and international trade.[4]

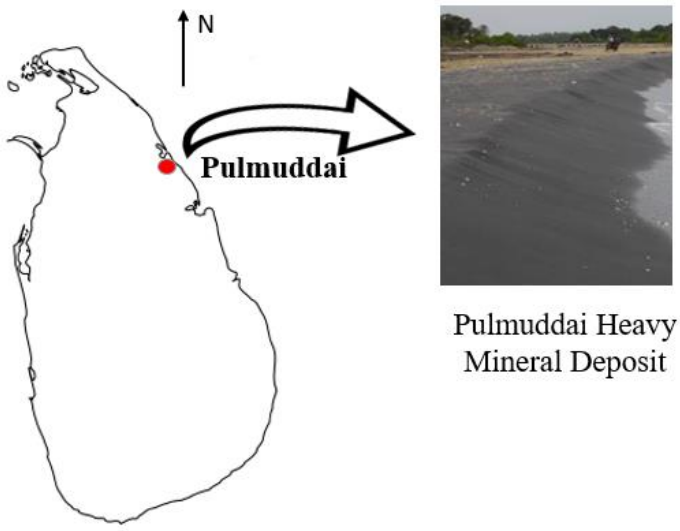

Figure 1.4: Pulmuddai heavy mineral deposit

The Pulmuddai beach sand deposit region showcases notable concentrations of ilmenite ($FeTiO_3$) and rutile (TiO_2). Furthermore, diverse beach mineral-sand deposits containing monazite, zircon, garnet, and ilmenite have been identified in various parts of the island and are presently subjected to export activities. Understanding the mineral richness of these deposits is crucial for both local industrial utilization and international trade.[4]

1.2 Introduction to Titanium Dioxide

Rutile, containing TiO_2, is a widely utilized substance, yet it is rarely found in its pure form in nature. In contrast, TiO_2 is abundant in ilmenite, leading research efforts to focus on titanium extraction from ilmenite. Two primary processes are employed for titanium production: the sulfate process and chlorination. In the sulfate process, ilmenite grains undergo dissolution in a sulfuric acid solution, forming titanium sulfate. This solution is then purified and subjected to hydrolysis to yield pure TiO_2. Despite its effectiveness, the sulfate process has drawbacks. It is time-consuming and generates undesirable byproducts such as unmarketable ferrous sulfate, spent sulfuric acid, and acidic wastewater for every ton of TiO_2 produced. If not managed properly, these byproducts can contribute to environmental concerns, emphasizing the need for sustainable and eco-friendly approaches in titanium production. [5][6]

Titanium dioxide serves as the most widely utilized white pigment and catalyst for photoactivity and bioactivity for the applications in pharmaceutical, cosmetic, paint and plastic industries as shown in Figure 1.5.

Figure 1.5: Products from Titanium Dioxide

Commercial production of TiO_2 relies on sulfate and chloride methods. In China, the sulfate technique, involving the dissolution of ilmenite in concentrated sulfuric acid, accounts for over 90% of the nation's titanium dioxide production. Cooling the titaniferous leach solution is done before hydrolysis to remove iron. The TiO_2 pigment is derived through the calcination of the processed materials. The challenge lies in removing Fe (II) from the leaching fluid, achievable through chilling. However, the hydrolytic slurry retains 30–40 g/l of ferrous ions, necessitating extensive washing to reduce the colored iron level to 20 ppm. This process generates significant

environmental concerns, producing between 100–250 tons of acid-containing washing water and 8 tons of wasted sulfuric acid (w/w) for every ton of TiO_2. The high concentration of ferrous sulfate complicates the evaporation of wasted acid, requiring limestone addition as a neutralizer before disposal, contributing to significant environmental challenges.[7]

Titanium complexes consist of cationic, anionic, and neutral forms in sulfuric acid solutions. According to theorists, a variety of extractants can extract titanium, including cation exchangers, anion exchangers, and neutral solvent reagents. The most promising application potential for acidic and neutral organophosphorus extractants can be found in literature reviews. Mono-(2-Ethylhexyl) phosphoric acid is one of the acidic organophosphorus extractants.

1.3 Objectives

- To separate the raw materials to obtain minerals from beach sand in Pulmuddai, Sri Lanka.
- To analyze the minerals for identify the mineral percentages and impurity percentages.
- To develop and optimize a method for the purification process for separated rutile from beach sand.
- To characterize the purified rutile for extraction of TiO_2

2. LITERATURE REVIEW

2.1 Titanium: Applications, Production, and Economic Implications

Titanium ranks as the Earth's ninth most abundant element, constituting about 0.6% of the crust. Predominantly found in ilmenite and mineral sand deposits, including rutile, anatase, leucoxene, and other titanium minerals such as brookite, perovskite, sphene, and geikielite. Beach sand contains different types of minerals with various properties outlined in Table 2-1.[8]

Table 2-1: Properties of beach sand minerals

Minerals	Physical properties
Ilmenite	Electrically conducting and strongly magnetic
Rutile	Electrically concluding and non-magnetic
Zircon	Non-conducting and non-magnetic
Monazite	Non-conducting and weakly magnetic
Quartz	Non-conducting and non-magnetic

Titanium products, renowned for their exceptional qualities, find broad applications in industries. Approximately 95% of the produced titanium is employed in manufacturing white titanium dioxide, a light-scattering pigment. TiO_2 pigments, distinguished by a high refractive index, deliver superior opacity and concealing power compared to alternatives. Notably, they showcase robust chemical resistance, thermal stability, and resilience against ultraviolet (UV) damage. Consequently, titanium dioxide pigments serve as pivotal raw materials in diverse sectors, encompassing paints, papers, printing inks, rubber, floor coverings, ceramics, medicines, and various chemical products.

In the aerospace sector, metallic titanium is extensively employed due to its corrosion resistance in chloride environments and high-temperature tolerance. Additionally, metallic titanium is utilized in the construction of water desalination facilities, chemical plants, and biomaterials.[9]

The demand for TiO_2 and titanium metal has led to an increase in TiO_2 pigment production, with a global capacity reaching 6.5 million tons. Similarly, the production

of titanium metal sponge has increased. However, the high manufacturing cost of metallic titanium limits its widespread use in various industries.

2.2 Processing Methods

The ilmenite concentrate derived from the vanadic titanomagnetite ore found in the Panxi area of Sichuan province is widely recognized as China's primary source of titanium dioxide. This particular ilmenite deposit holds over 90% of China's titanium resources and more than 35% of the world's, making it a strategically important reserve of titanium. Given the high content of iron (Fe) and titanium dioxide (TiO_2) in this rock-type titanium ore, an advanced processing method involving gravity separation, magnetic separation, flotation, and even leaching processes is employed to extract the valuable TiO_2 and Fe components.[10]

Processing low-quality titanium sands presents challenges due to their lower mineral grade. These sands, containing fewer essential minerals, diverge from the processing methods applied to rock-type ores. Despite ranking as China's second-largest titanium deposit, low-grade titanium sands have gained importance for manufacturing ilmenite concentrate. This shift results from the depletion of high-grade titanium ores and increased demand for titanium dioxide. However, their low grade and intricate association with gangue minerals pose difficulties for conventional processing techniques.

Despite their abundance, the practical and large-scale utilization of these low-quality titanium sands remains limited. The complexities arising from their lower grade and mineral interconnection demand innovative approaches for efficient processing. Enhancing the utilization of these resources requires overcoming the existing limitations through advanced technologies and methodologies. In conclusion, the significance of low-quality titanium sands in the production of ilmenite concentrate is acknowledged. Yet, their practical application faces challenges, emphasizing the need for further research and technological advancements in titanium processing.[11][12]

In the conventional processing of titanium sands, a series of intricate steps are employed to extract valuable minerals. Initially, the titanium sands undergo grinding and classification within a closed circuit. The excess material is then carefully processed through a separation procedure utilizing numerous spirals. These specialized spirals effectively segregate minerals like silica, silicate, aluminate, and others from the mixture. Importantly, a substantial portion of titanium middlings, the intermediate product of this process, is reintroduced into the system. This middlings material undergoes additional grinding and classification in various circuits to ensure optimal liberation.

Following this, the concentrated material derived from the spirals undergoes a meticulous separation process. This involves categorizing the material into two main groups: strongly magnetic titanomagnetites and weakly magnetic ilmenites. Achieved through a method known as low-intensity magnetic separation (LMS), this step is crucial for refining the concentrate. In specific scenarios, electrostatic separation may be applied to further purify the ilmenite concentrate. It's essential to highlight that the recovery of separated titanium minerals exhibits considerable variation, a factor determined by their distinct physical characteristics.[13]

Vanadium titanomagnetite ore stands as a valuable reservoir of iron, vanadium, and titanium, and the Panzhihua-Xichang area in China holds a prominent position for its copious vanadium titanomagnetite deposits. These deposits are estimated to house a staggering 9.66 billion tons of ore, boasting 11.6% vanadium and 35.17% titanium. Within this region, intricate processing procedures are employed to derive essential products such as ilmenite concentrate, vanadium titanomagnetite concentrate, and various other minerals from the vanadium titanomagnetite ore.

The predominant method historically used for extracting iron and vanadium from the vanadium titanomagnetite concentrate involves the blast furnace technique. This process targets the vanadium titanomagnetite concentrate, which holds approximately 52% titanium and 89% vanadium. However, the conventional approach doesn't effectively harness the potential of titanium found in the titanium-bearing blast furnace slag, featuring a TiO_2 content ranging between 22-25 wt.%. Numerous strategies have

been explored to optimize the utilization of the titanium resource within the vanadium titanomagnetite concentrate. These include sodium salt roasting-direct reduction-electric furnace smelting and direct reduction-magnetic separation. Despite promising outcomes in laboratory settings, these technologies have not yet transitioned into commercialization. [14] [15]

Conversely, the direct reduction-electric furnace smelting process has achieved successful commercialization in South Africa and New Zealand, owing to its large-scale production capabilities and mature vanadium recovery technology within molten iron. This method is considered more environmentally friendly compared to traditional blast furnaces. Notably, the titanium-bearing electric furnace slag (TEFS) produced through direct reduction-electric smelting contains a significantly higher concentration of TiO_2 compared to titanium-bearing blast furnace slag. Consequently, the effective extraction of titanium from TEFS holds paramount importance for advancing direct reduction-electric furnace smelting techniques and ensuring the efficient utilization of vanadium titanomagnetite concentrate.

2.3 Beach Sand Deposits

Beach sand stands as a globally significant reservoir of titanium minerals, and while hard rock sources in Canada and Norway also contribute to ilmenite extraction, Sri Lanka boasts a long-standing history of being recognized for its natural concentrations of titanium-bearing mineral sands, particularly high-purity ilmenite and rutile, a recognition dating back to 1903. The northeast coast of Sri Lanka, near Pulmuddai, has been a focal point for mining since 1958, harboring the largest deposits, and it extends along a 7.2-kilometer stretch of coastline with an average width of 50 meters, reaching a maximum width of 250 meters. Situated on Precambrian crystalline rock with minimal overburden, the deposit spans an area of 3.2 square kilometers. [4]

Distinguished by its high-grade composition, the deposit comprises approximately 70-72% ilmenite, 8-10% zircon, 8-10% rutile, 1-1.5% sillimanite, and 0.3-0.5% monazite. These mineral proportions reflect a prevalence of ilmenite, zircon, rutile, sillimanite, and monazite. These mineral-rich sands along Sri Lanka's beaches serve as a valuable resource for extracting titanium minerals on a commercial scale.

In the mineral sands industry, the treatment of heavy mineral concentrates often involves high-intensity magnetic separation. At the Pulmuddai factory in Sri Lanka, wet magnetic separation is employed to extract ilmenite from the concentrates. Additionally, various plant processes utilize dry magnetic separation, particularly for the recovery of titanium-bearing minerals like ilmenite and leucoxene from heavy mineral concentrates.[4][16]

The economic and industrial significance of these deposits is underscored by their long history of extraction and their contribution to the global supply of titanium minerals. Sri Lanka's strategic position as a source of high-quality titanium-bearing mineral sands has not only fueled its domestic industries but has also played a role in the broader landscape of global titanium production. The continued exploration and sustainable extraction of these resources will likely contribute to meeting the growing demand for titanium minerals in various industrial applications.

The value of a beach sand deposit extends beyond its potential for separation processes; it hinges significantly on the intricate interplay of mineralogical characteristics. Sri Lanka's Geological Survey Department has undertaken extensive research over the past few decades, delving into the distribution and mineralogy of beach sand deposits across the country. Notably, studies have honed in on the offshore region adjacent to the actively exploited Pulmoddai beach deposit, unraveling the mineral composition and properties of these deposits. Such endeavors provide crucial insights, not only into the geology but also into the economic viability of these resources, shaping the strategies for their extraction.[17][18]

Within this context, a notable gap has emerged in the comprehensive analysis of the mineralogical and chemical facets of Sri Lanka's beach sand deposits, coupled with an absence of dedicated inquiries into the recovery of titanium-bearing minerals via magnetic separation. Addressing this void, our study unfolds with the specific objective of scrutinizing the mineralogical and chemical traits of a chosen beach sand deposit in Sri Lanka. Concurrently, we aspire to explore the practical application and optimization of diverse magnetic separators. This dual-pronged approach aims to

bolster the effectiveness, efficiency, and cost-effectiveness of the titanium recovery process from the deposit.

Embarking on a meticulous analysis of the mineralogical and chemical intricacies of the beach sand deposit, our study seeks to unravel its composition comprehensively, with a specific focus on identifying the presence of titanium-bearing minerals. Subsequent stages involve the strategic application and optimization of various magnetic separators, each tailored to enhance the recovery process. The overarching goal is twofold: to refine the efficiency of titanium recovery and augment the overall yield of valuable titanium resources sourced from Sri Lanka's beach sand deposit.

In essence, this research aims to bridge existing knowledge gaps, offering a holistic understanding of the beach sand deposit's potential and facilitating advancements in recovery methodologies. By integrating geological insights with cutting-edge separation technologies, the study strives to pave the way for a more efficient and economically viable extraction process from Sri Lanka's beach sand deposits.[4][19]

3. METHODOLOGY

3.1 Materials and Apparatus

The starting material for this study was beach sand sourced from Pullmuddai, Sri Lanka, enriched with ilmenite and rutile. Hydrochloric acid (HCl) with a 35.4% assay was procured from Sigma Aldrich Company to facilitate the extraction and purification process. Various equipment, including a high-tension separator, Wilfley table, Humphrey spiral, and Magnetic separator, were utilized to play crucial roles in concentrating the mineral samples. The analysis of samples involved the use of GENESYS 10S Series UV-Visible Spectrophotometer and Scanning Electron Microscopy. This comprehensive suite of materials and apparatus formed the foundation for the experimental procedures, ensuring accurate testing and analysis of the mineral samples.

3.2 Separation Process

In the preliminary stages of the experiment, beach sand samples were screened to eliminate shells and undesirable materials. Subsequently, one sample was subjected to the milling process, while the other remained untouched. The identification of the sample with the highest rutile mineral yield was facilitated by employing a magnetic separator as shown in Figure 3.1.[18][20]

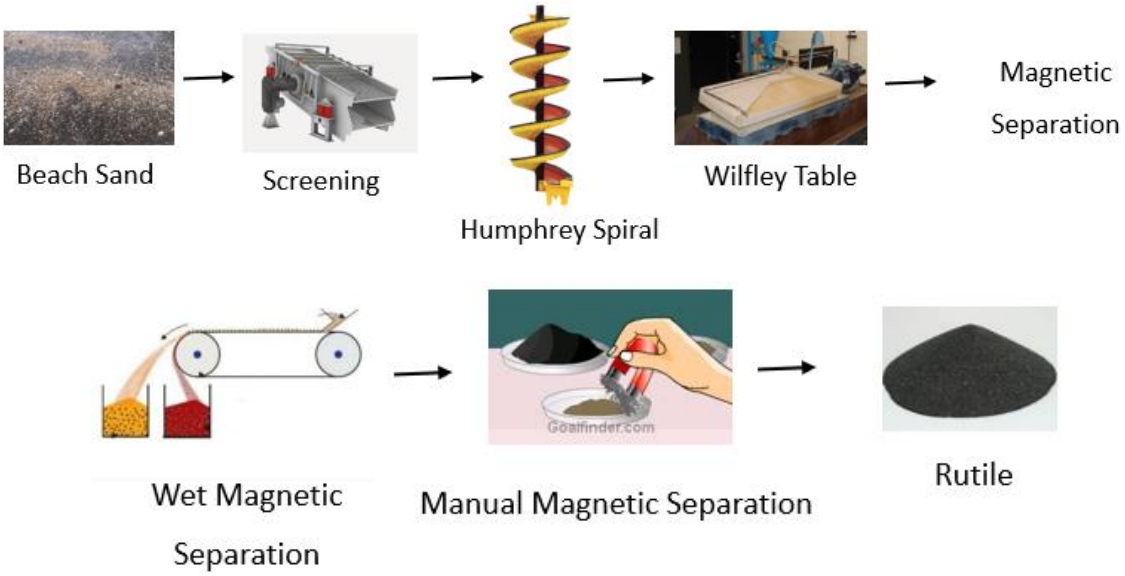

Figure 3.1: Separation Procedure

The milling process revealed an increased rutile yield in the respective sample, leading to the decision to employ milled samples for the extraction of high-density mineral sand using a Humphrey spiral separator. The elimination of tailings occurred, and the substantial fraction underwent concentration using a Wilfley table. Following this, a wet magnetic separator was employed to extract non-magnetic minerals.

However, achieving the desired non-magnetic concentrate required an additional step of tabling the concentrate to separate light minerals effectively. The final separation of rutile from the yielded sample was accomplished using a high-tension separator due to its conductivity, as depicted in Figure 3.2. This intricate yet systematic process aimed to optimize rutile extraction and enhance the overall efficiency of the mineral concentration process.[21]

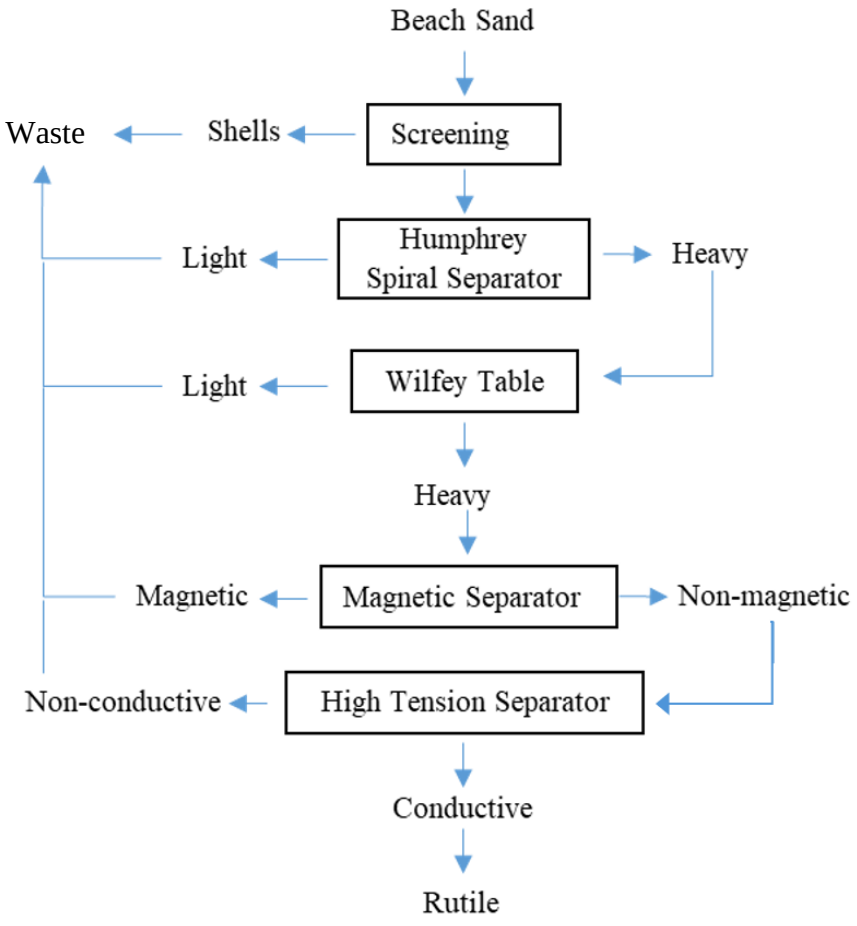

Figure 3.2: Beach Sand Separation Process

3.3 Purification Process

After the separation process, rutile samples were sieved to analyze particle size and distribution. Three categorized samples were identified using the size distribution of the initial sample as shown in Figure 3.3. Subsequent EDX analysis of rutile samples revealed mineral composition and impurity percentages. The sample with a particle size less than 150 µm exhibited the highest rutile concentration and was selected for the purification process. Iron removal from rutile was achieved by leaching the mixture with hydrochloric acid (HCl), utilizing two distinct methods to enhance precision in the purification process. This meticulous approach ensures the efficiency of the purification process, guaranteeing a high-quality rutile product for further applications.

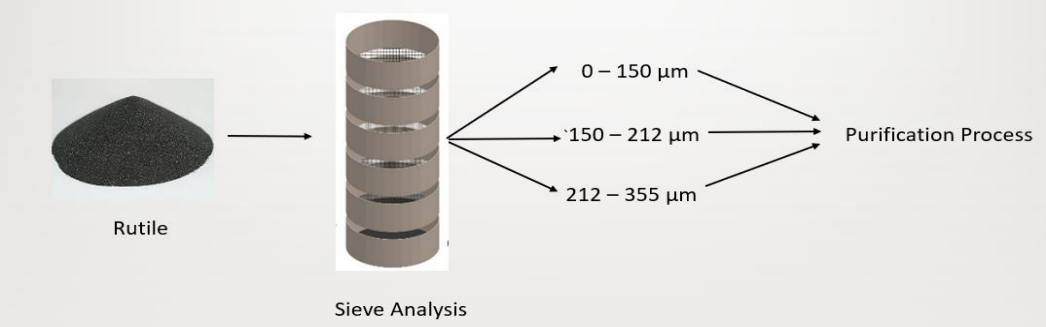

Figure 3.3: Process of Sieve Analysis

The purification process was carried out under two methods to achieve the maximum yield in removing iron content from the rutile.

3.4 Method 01: Purification Process

The purification process was done varying by different variables with different parameters for the separated minerals as shown in Figure 3.4. Those variables were,

- Particle Size
- Temperature
- Time
- Acid Type
- Acid concentration

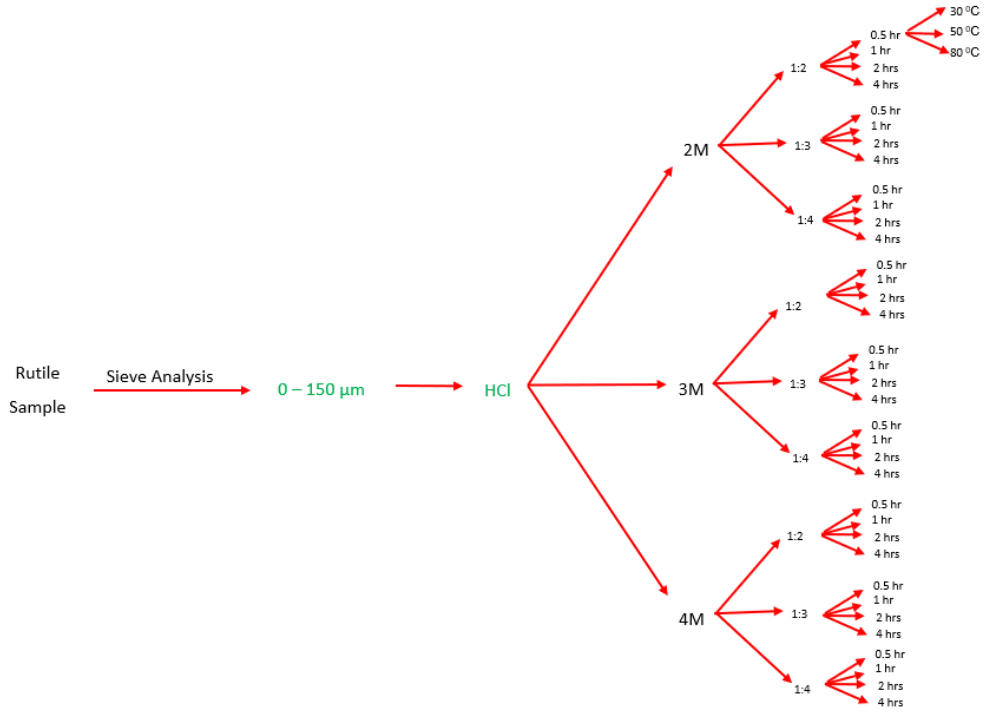

Figure 3.4: Variation of the Testing Parameters in Method 01

Those variables were changed with the different parameters as mentioned below.

Particle Size (µm)

- 0 – 150
- 150 – 212
- 212 – 355

Acid Concentration (M)

- 2
- 3
- 4

Temperature (^{0}C)

- 30 ± 5
- 50 ± 5
- 80 ± 5

Time (Hours)

- 0.5
- 1
- 2
- 4

S/L Ratio

- 1:2
- 1:3
- 1:4

Acid Type

- HCl

Initially analyzed samples were leached with HCl by varying reaction times as 0.5, 1, 2, and 4 hours with a 1:2 solid-to-liquid ratio and 2M HCl concentration while maintaining different temperatures. The same process was repeated while changing the parameters as shown in the below diagram according to the results obtained from the initial analysis. Acid was always HCl and the particle size was maintained in the range of 0 – 150 µm. Concentration, S/L ratio, reaction time and temperature were change according to preidentified parameters. After each test, results were analyzed using same method to identify the remain iron percentage and calculated the iron reduction percentage. Finally, all the details were graphed and maximum iron reduction percentages were identified and summarized.

After analyzing the results from method 01, method 02 was defined as reducing initial particle size and increasing the separation process with the magnetic separation process. Then with the results of the previous method, different methods were identified to get maximum output for removal of the iron content.

3.5 Method 02: Purification Process

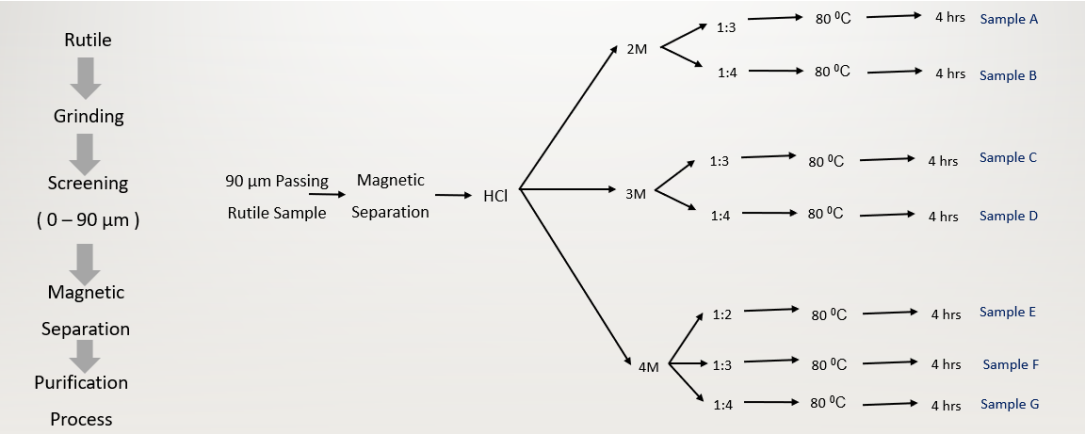

Figure 3.5: Variation of the Testing Parameters in Method 02

After this leaching process, samples were analyzed to observe the maximum iron-reducing sample.

3.6 Characterization

After each purification process, leached samples were filtered to get the solutions for tests with UV Visible spectrophotometer to identify the sample, which has the maximum dissolution of iron. The optimized condition was identified for each process by analyzing the UV visible spectrophotometer data. Those optimized conditioned samples were dried and tested with EDX to analyze the remain impurity weight percentages.

4. RESULTS AND DISCUSSION

The initial raw mineral sample was sieved after the screening and separation process to identify the particle distribution of the sample as shown in Table 4.1 and converted to a cumulative graph shown in Figure 4.1.

Table 4.1: Sieve Analysis Data (Cumulative Value)

Reference Number	Particle Size (µm)	Cumulative Weight (g)	Cumulative Weight Percentage (%)
1	> 500	2.0	0.04
2	> 425	4.0	0.08
3	> 355	11.5	0.23
4	> 300	42.5	0.85
5	> 250	823.0	16.49
6	> 212	1577.0	31.60
7	> 180	2963.0	59.38
8	> 150	3426.5	68.67
9	> 125	4525.5	90.69
10	> 90	4879.5	97.79
11	> Pan	4990.0	100.00

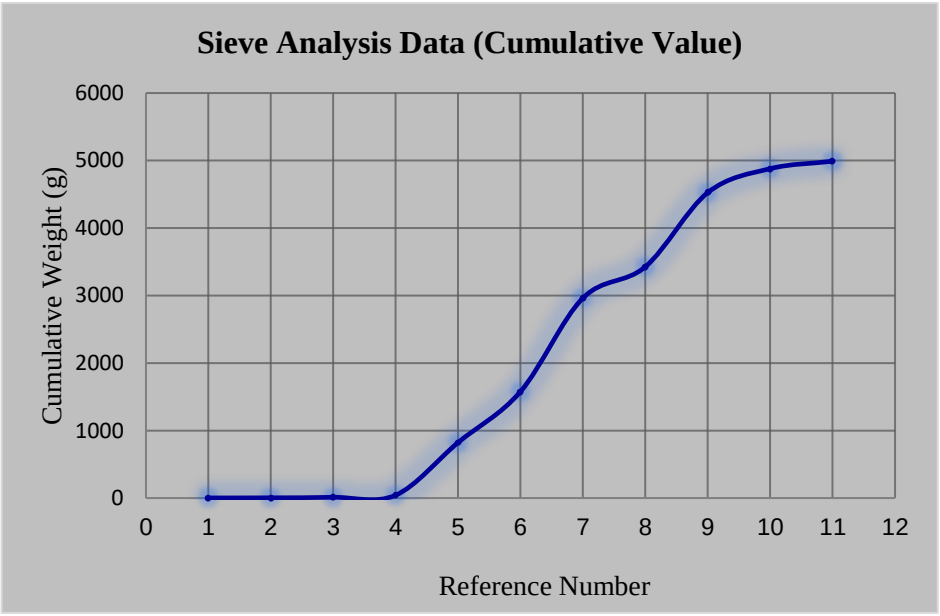

Figure 4.1: Cumulative Graph for the Sieve Analysis

More than 99% of the sample below the 355 µm range and divided into three groups with the average cumulative value of 30% wt.

1. 0 – 150 µm
2. 150 – 212 µm
3. 212 – 355 µm

Before separation to three categories, initial samples were analyzed for identification of the mineral content using EDX as shown in Figure 4-2 and obtained results are in Table 4.2.

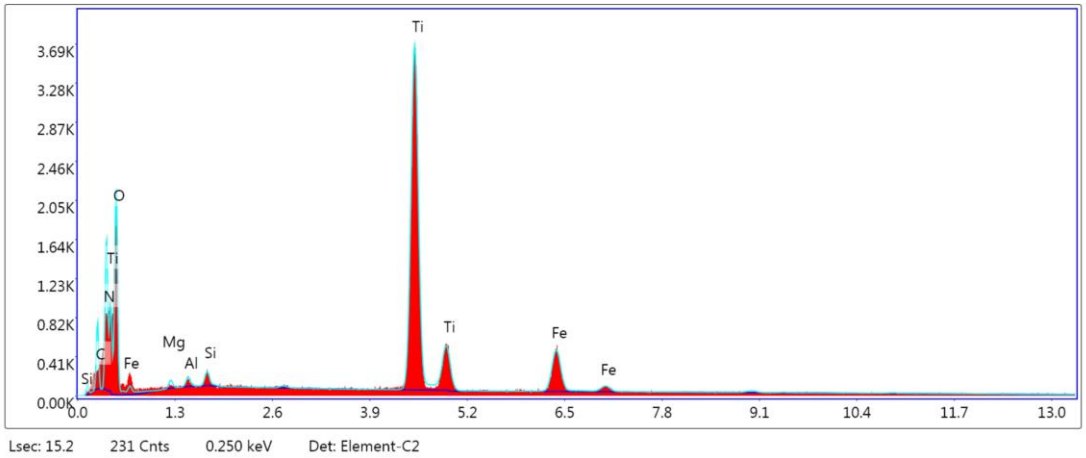

Figure 4.2: EDX results for initial mineral sample

Table 4.2: EDX Results for initial sample

Element	Weight %
C	3.18
N	1.89
O	40.26
Al	0.63
Si	0.88
Mg	0.01
Ti	43.58
Fe	9.57

The initial sample shows sand minerals contain with high amount of titanium with less amount of iron (Fe). It contains also fewer amounts of aluminum, silicon and carbon with other elements. As shown in Table 4.3, iron can be identified as the major impurity of the mineral sample. By leaching process, iron can be removed while leaching the aluminum.

After categorizing the mineral using the sieve analyzing method, each sample was tested for analyzing the mineral content. iron was the major impurity, amount of present in the mineral sand by weight percentage was summarized as shown in Table 4.3.

Table 4.3: Summarized EDX data for different ranges

Particle Size (μm)	**Ti (Wt %)**	**Fe (Wt %)**
0 – 150	43.04	16.91
150 – 212	43.98	10.18
212 – 355	42.83	9.95

The highest amount of iron by weight percentage is contained in the 0 – 150 μm sample category and all the samples have with average amount of titanium content in oxide form. Due to the highest amount of iron in the lowest particle size sample, used for the purification process.

According to the identified two methods, method 01 and 02 followed respectively.

4.1 Method 01

Purification Process (0 – 150 μm with HCl)

The purification process was conducted according to Method 01 in Figure 4.3, with variations in concentration, S/L ratio, reaction time, and temperature. The results obtained from the EDX tests after the purification process were used to plot graphs

showing iron reduction in relation to the variations in temperature, S/L ratio, concentration, and time.

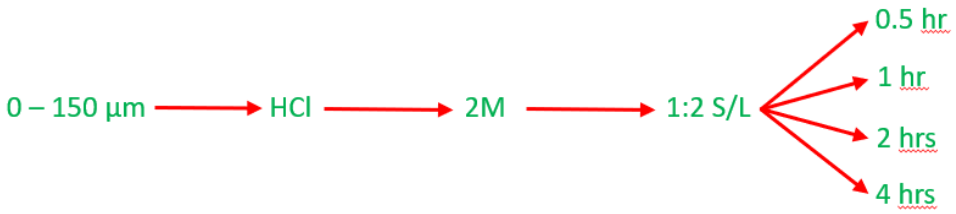

Figure 4.3: Purification process for 2M concentration sample

The S/L ratio, time, and temperature were varied while the acid concentration was maintained at 2M. The sample was initially tested to obtain the initial iron percentage and was tested again after the purification process to calculate the iron reduction percentage. The data obtained for the tested samples at 2M concentration is shown in Table 4.4.

Table 4.4: Variation with temperature & time (Concentration 2M & 1:2 S/L Ratio)

Acid Concentration	S/L Ratio	Time (hrs)	Temperature (^{0}C)	Initial Fe % (wt)	Final Fe % (wt)	Fe reduction % (wt)
2M	1:2	0.5	30	16.91	15.39	8.99
			50		14.82	12.36
			80		14.46	14.49
		1	30		14.65	13.36
			50		14.27	15.61
			80		13.85	18.10
		2	30		14.95	11.59
			50		14.01	17.15
			80		13.12	22.41
		4	30		14.72	12.95
			50		12.84	24.07
			80		12.92	23.60

The obtained test data was revealed to show a significant correlation between temperature variations and iron content reduction. As temperatures were increased, the reduction of iron content was observed to follow suit, demonstrating a dynamic relationship over the course of the experiment. A comparative analysis between the temperatures of 30°C and 80°C was underscored as revealing a noteworthy observation, indicating a substantial increase of almost 100% in iron reduction. Valuable insights into the intricate dynamics of iron reduction were offered by this temperature-dependent trend, and the importance of temperature control in influencing the desired outcomes in the reduction process was underscored.

Similarly, an analogous pattern was observed to emerge in the 1:3 S/L ratio segment of the experiment as the temperature was increased, as shown in Table 4.5.

Table 4.5: Variation with temperature & time (Concentration 2M & 1:3 S/L Ratio)

Acid Concentration	S/L Ratio	Time (hrs)	Temperature (^{0}C)	Initial Fe % (wt)	Final Fe % (wt)	Fe reduction % (wt)
2M	1:3	0.5	30	17.00	16.01	5.82
			50		14.98	11.88
			80		14.72	13.41
		1	30		14.86	12.59
			50		14.11	17.00
			80		13.64	19.76
		2	30		14.62	14.00
			50		14.13	16.88
			80		13.74	19.18
		4	30		14.53	14.53
			50		12.34	27.41
			80		12.02	29.29

The data was indicated to show a notable 50% improvement in iron reduction at 80°C compared to the observations at 30°C. The reproducibility of the observed temperature-dependent phenomenon was underscored by the comparative analysis, with the consistency of the relationship between temperature and iron reduction across different experimental conditions being emphasized. The notion that temperature played a pivotal role in influencing iron reduction processes and their outcomes was further supported.

The findings from the conducted experiment were shown to clearly reveal the significant impact of temperature and time on the iron reduction process, especially within the context of a specific solid-to-liquid (S/L) ratio and acid concentration, as shown in Table 4.6.

Table 4.6: Variation with temperature & time (Concentration 2M & 1:4 S/L Ratio)

Acid Concentration	S/L Ratio	Time (hrs)	Temperature (^{0}C)	Initial Fe % (wt)	Final Fe % (wt)	Fe reduction % (wt)
2M	1:4	0.5	30	15.39	14.23	7.54
			50		13.52	12.15
			80		13.27	13.78
		1	30		13.23	14.04
			50		13.02	15.40
			80		12.41	19.36
		2	30		13.14	14.62
			50		12.76	17.09
			80		11.98	22.16
		4	30		13.49	12.35
			50		11.41	25.86
			80		10.92	29.04

The observed data was consistently illustrated to show a progressive increase in the percentage of iron reduction, with the intricate interplay between time, temperature, and the chosen S/L ratio being underscored. This synchronous elevation in iron reduction, influenced by both time and temperature variables, was accentuated as highlighting the nuanced dynamics at play during the experimental conditions. The discernible trends were shown to shed light on the interconnected roles these factors played in shaping the effectiveness of the iron reduction process under the specified experimental parameters.

As shown in Figure 4.4, the following graphs were plotted with the variables for 2M concentration, and the maximum iron reduction percentages were observed after the analyzing process.

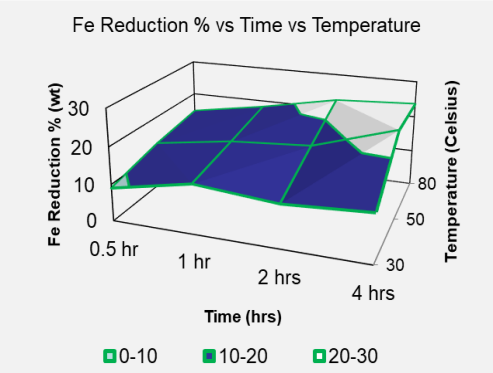

(S/L ratio 1:2)

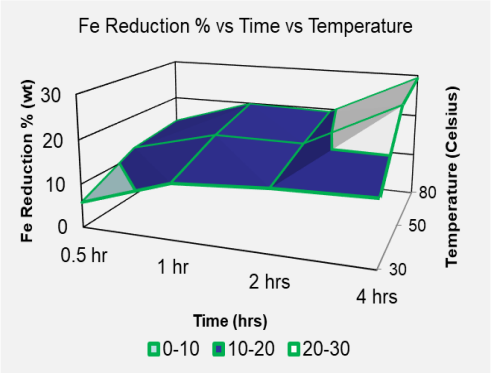

(S/L ratio 1:3)

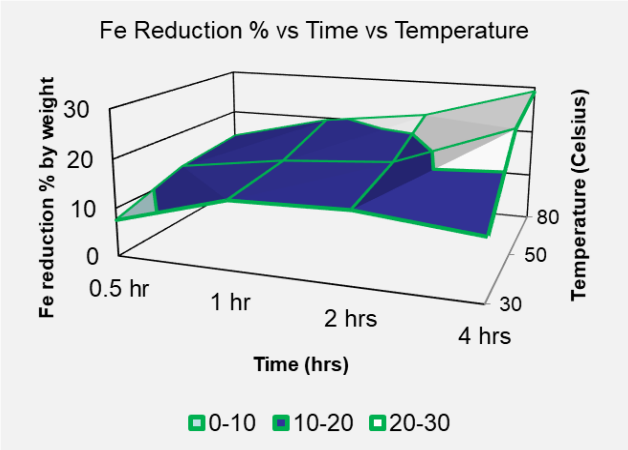

(S/L ratio 1:4)

Figure 4.4: Variation with temperature & time (Concentration 2M)

The 3-D graphs were offered to provide a detailed overview of the patterns evident in the accompanying tables. The graphs were depicted to show how alterations in parameters influenced the percentage of iron reduction. Importantly, the experiment was highlighted as presenting challenges linked to elevating temperature and regulating acid concentration. Within these constraints, the highest attainable iron reduction was limited to 29%. This restriction was underscored as illustrating the delicate equilibrium necessary for optimizing temperature and acid concentration, ensuring an efficient iron reduction process under the defined experimental conditions. The findings were stressed as emphasizing the importance of a nuanced strategy toward these variables to fully exploit the potential of the reduction process while acknowledging existing limitations.

The same procedure was followed by varying different parameters, as shown in Table 4.7, and the iron reduction percentages were calculated and plotted with graphs for analysis.

Table 4.7: Variation with temperature & time (Concentration 3M & 1:2 S/L Ratio)

Acid Concentration	S/L Ratio	Time (hrs)	Temperature (^{0}C)	Initial Fe % (wt)	Final Fe % (wt)	Fe reduction % (wt)
3M	1:2	0.5	30	14.12	13.51	4.32
			50		12.14	14.02
			80		11.01	22.03
		1	30		12.95	8.29
			50		12.03	14.80
			80		10.54	25.35
		2	30		12.12	14.16
			50		11.85	16.08
			80		10.23	27.55
		4	30		11.98	15.16
			50		10.65	24.58
			80		9.14	35.27

Based on the conducted tests under a 3M acid concentration, as shown in Table 4.7, optimal conditions for iron reduction were identified by employing a 1:2 solid-to-liquid (S/L) ratio over a duration ranging from 30 minutes to 4 hours and varying temperatures from 30 to 80°C. The maximum reduction of iron, amounting to 35.27%, was achieved under a temperature of 80°C for a duration of 4 hours. The significance of temperature and duration in maximizing iron reduction under the specified experimental parameters was highlighted by these findings.

It was identified that the minimum iron reduction occurred within the initial 30 minutes at a temperature of 30°C. The maximum output of 29.72% was attained with a 1:2 solid-to-liquid (S/L) ratio and a 2M acid concentration. A comparable result of nearly 27.55% was achieved with a 1:3 S/L ratio under a 3M concentration, maintaining a 2-hour duration at 80°C.

The same procedure was followed for the 1:2 ratio along with 3M concentration, as shown in Table 4.8.

Table 4.8: Variation with temperature & time (Concentration 3M & 1:3 S/L Ratio)

Acid Concentration	S/L Ratio	Time (hrs)	Temperature (^{0}C)	Initial Fe % (wt)	Final Fe % (wt)	Fe reduction % (wt)
3M	1:3	0.5	30	14.56	13.54	7.01
			50		12.84	11.81
			80		11.35	22.05
		1	30		12.84	11.81
			50		12.17	16.41
			80		10.87	25.34
		2	30		12.06	17.17
			50		11.63	20.12
			80		10.11	30.56
		4	30		11.89	18.34
			50		10.87	25.34
			80		8.97	38.39

The data in Table 4.8 was shown to clearly illustrate a significant boost in iron reduction percentages when comparing the results to those of the 1:2 ratio under a 3M concentration. As the experiment progressed, a steady rise in iron reduction was observed, peaking at 38.39% during the 4-hour period at 80^{o}C. Interestingly, even in a shorter 2-hour duration at the same temperature, iron reduction remained consistently above 30%.

The impact of a 1:4 S/L ratio alongside heightened acid concentrations was investigated, revealing a significant enhancement in the test results, as shown in Table 4.9.

Table 4.9: Variation with temperature & time (Concentration 3M & 1:4 S/L Ratio)

Acid Concentration	S/L Ratio	Time (hrs)	Temperature (^{0}C)	Initial Fe % (wt)	Final Fe % (wt)	Fe reduction % (wt)
3M	1:4	0.5	30	15.78	14.01	11.22
			50		12.66	19.77
			80		12.14	23.07
		1	30		12.97	17.81
			50		11.97	24.14
			80		10.35	34.41
		2	30		11.98	24.08
			50		12.04	23.70
			80		10.85	31.24
		4	30		12.75	19.20
			50		10.47	33.65
			80		9.41	40.37

However, a markedly higher margin was not demonstrated by this improvement when compared with the preceding parameters. The pinnacle of iron reduction, registering at 40.37%, was denoted as showing an approximate 5% increment from the antecedent conditions, with only the S/L ratio being altered. The constancy observed in iron reduction across diverse parameters was signified as illustrating the inherent resilience of the process. Despite modifications in the S/L ratio and acid concentration, a steadfast consistency in the overarching effect on iron reduction was maintained.

The subsequent graphs in Figure 4.5 were generated using data acquired from altering the concentration to 3M with different S/L ratios.

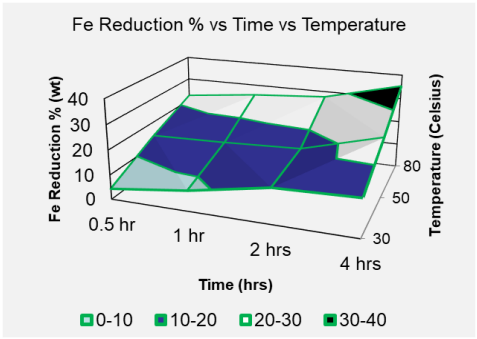

(S/L ratio 1:2)

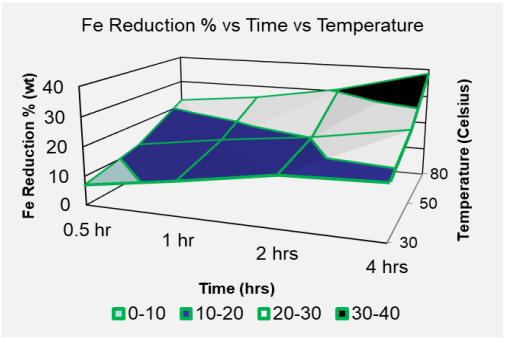

(S/L ratio 1:3)

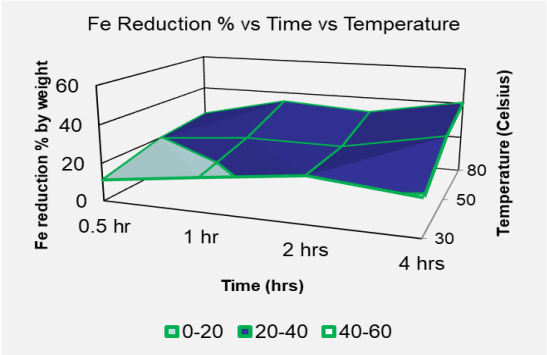

(S/L ratio 1:4)

Figure 4.5: Variation with temperature & time (Concentration 3M)

Subsequently, another sample was tested with a 4M concentration using the same parameters that were employed for the 2M and 3M concentrated samples, as shown in Table 4.10.

Table 4.10: Variation with temperature & time (Concentration 4M & 1:2 S/L Ratio)

Acid Concentration	S/L Ratio	Time (hrs)	Temperature (^{0}C)	Initial Fe % (wt)	Final Fe % (wt)	Fe reduction % (wt)
4M	1:2	0.5	30	17.48	15.24	12.81
			50		14.95	14.47
			80		13.85	20.77
		1	30		14.98	14.30
			50		13.65	21.91
			80		12.98	25.74
		2	30		15.84	9.38
			50		14.25	18.48
			80		12.56	28.15
		4	30		14.78	15.45
			50		13.41	23.28
			80		11.24	35.70

The data was indicated to show an increase in iron reduction when the 1:2 ratio was compared with various acid concentrations. Specifically, under the 1:2 ratio, the maximum iron reduction observed at 30°C within a 30-minute timeframe with a 4M concentration was found to be nearly equivalent to the iron reduction achieved at 1M concentration with a 4-hour duration under 30°C.

The extraction procedure was followed with a 4M concentration and a 1:3 S/L ratio, yielding the optimum results as mentioned in Table 4.11.

Table 4.11: Variation with temperature & time (Concentration 4M & 1:3 S/L Ratio)

Acid Concentration	S/L Ratio	Time (hrs)	Temperature (^{0}C)	Initial Fe % (wt)	Final Fe % (wt)	Fe reduction % (wt)
4M	1:3	0.5	30	16.95	15.01	11.45
			50		14.56	14.10
			80		13.99	17.46
		1	30		14.85	12.39
			50		13.96	17.64
			80		12.47	26.43
		2	30		14.21	16.17
			50		14.01	17.35
			80		13.65	19.47
		4	30		14.65	13.57
			50		13.21	22.06
			80		11.04	34.87

When the 1:2 ratio was compared with the 1:3 ratio under the same 4M concentration, the results were found to nearly overlap, indicating that the effect of the S/L ratio was significantly diminished at higher concentrations. The maximum iron reduction, reaching 34.87%, was achieved at the highest variable values, as shown in Table 4.11. This suggested that, under increased acid concentration, the influence of the S/L ratio became less pronounced, emphasizing the dominant impact of acid concentration on the iron reduction process.

The final extraction procedure under Method 01 was conducted with a 4M concentration and a 1:4 ratio, resulting in the data presented in Table 4.12.

Table 4.12: Variation with temperature & time (Concentration 4M & 1:4 S/L Ratio)

Acid Concentration	S/L Ratio	Time (hrs)	Temperature (^{0}C)	Initial Fe % (wt)	Final Fe % (wt)	Fe reduction % (wt)
4M	1:4	0.5	30	15.84	13.24	16.41
			50		12.95	18.24
			80		11.88	25.00
		1	30		12.92	18.43
			50		11.32	28.54
			80		10.82	31.69
		2	30		13.07	17.49
			50		11.41	27.97
			80		10.32	34.85
		4	30		12.85	18.88
			50		10.95	30.87
			80		10.37	34.53

The analyzed test results indicated that iron dissolution was stabilized at approximately 35% when exposed to leaching for 2 hours and 4 hours under a 1:4 S/L ratio, as shown in Table 4.12. This was revealed to be a lower iron reduction compared to the 3M concentration with the same S/L ratio. The data highlighted that the leaching process achieved a maximum reduction of around 40%, showcasing the impact of both time and S/L ratio on iron dissolution.

The results were summarized through 3D graphs, as shown in Figure 4.6, with various S/L ratios depicted under identical time and temperature conditions. These graphs visually represented the fluctuation in iron reduction concerning different parameters.

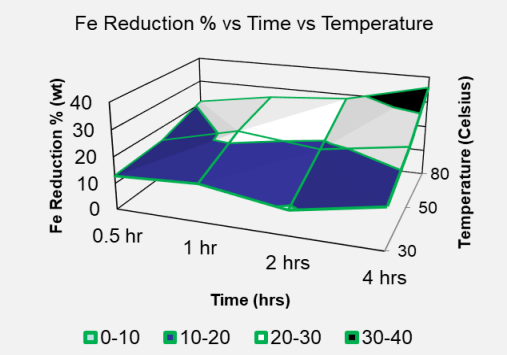

(S/L ratio 1:2)

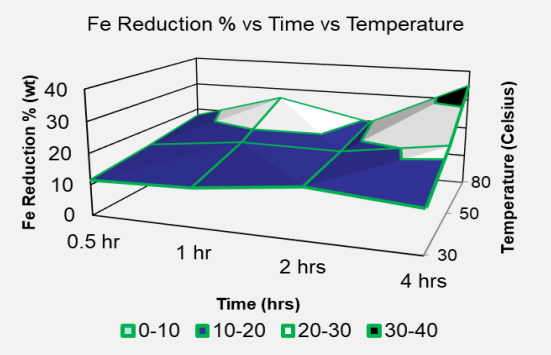

(S/L ratio 1:3)

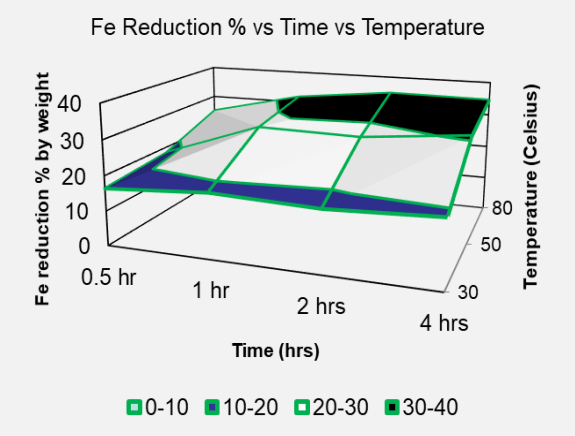

(S/L ratio 1:4)

Figure 4.6: Variation with temperature & time (Concentration 4M)

The above results were acquired by altering acid concentration, S/L ratio, temperature, and time during the test. A comprehensive analysis was conducted using 3D graphs to facilitate a thorough examination, allowing for the identification of iron content reduction in relation to these parameters. The subsequent section was outlined to present the highest iron reduction results based on the findings extracted from the graphs, providing valuable insights into the intricate relationship between these variables.

Highest Fe Reduction with 2M Concentration

1. 1:3 S/L Ratio, 80 ^{0}C ± 5. 4 hrs

   Fe reduction: 29.29 % (wt)

2. 1:4 S/L Ratio, 80 ^{0}C ± 5, 4 hrs

   Fe reduction: 29.04 % (wt)

Highest Fe Reduction with 3M Concentration

1. 1:3 S/L Ratio, 80 ^{0}C ± 5, 4 hrs

   Fe reduction: 38.39% (wt)

2. 1:4 S/L Ratio, 80 ^{0}C ± 5, 4 hrs,

   Fe reduction: 40.37 % (wt)

Highest Fe Reduction with 4M Concentration

1. 1:2 S/L Ratio, 80 ^{0}C ± 5, 4 hrs

   Fe reduction: 35.70 % (wt)

2. 1:3 S/L Ratio, 80 ^{0}C ± 5, 4 hrs

   Fe reduction: 34.87 % (wt)

3. 1:4 S/L Ratio, 80 ^{0}C ± 5, 4 hrs

   Fe reduction: 34.53 % (wt)

All the highest iron reductions were obtained with a 4-hour reaction time, and it was noted that increasing the concentration allowed the S/L ratio to be reduced. As the concentration increases, the amount of HCl in the content rises, which enhances the reduction of iron content while maintaining a lower solid-to-liquid ratio. When comparing the 3M concentration with the 2M concentration, the 2M concentration showed around 30% iron reduction at the highest values, whereas the 3M concentration showed around 40% iron reduction with the same parameters except for concentration.

The primary cause of this difference was attributed to the amount of HCl in the content rather than other factors. When comparing the 3M with the 4M concentration, the 4M concentration resulted in a lower iron reduction of approximately 35%, but this difference was not significantly larger than that with the 3M concentration. After analyzing the previous UV spectrophotometer data and the above results, it was observed that iron reduction reaches saturation with increased concentration but shows a smaller increase with additional time.

However, the above results confirmed that the maximum iron reduction can be achieved up to 40% with the current method, and it is suggested that the method should be upgraded or changed to obtain higher iron reduction. The following method was developed by reducing the particle size of the raw material to achieve a larger surface area for reaction with the chemicals.

In Method Two, samples were sieved using a 90 µm passing sieve to obtain fine particles. The obtained fine particles were then purified using the optimum conditions derived from Method One. The samples were labeled from A to G, with the purification process parameters as follows:

- Sample A and B were purified according to the highest iron reduction parameters obtained from the 2M concentration.
    - Sample A - 1:3 S/L Ratio, 80 ^{0}C ± 5. 4 hrs
    - Sample B - 1:4 S/L Ratio, 80 ^{0}C ± 5, 4 hrs
- Sample C and D underwent purification with the highest iron reduction parameters obtained from the 3M concentration.
    - Sample C – 1:3 S/L Ratio, 80 ^{0}C ± 5, 4 hrs
    - Sample D – 1:4 S/L Ratio, 80 ^{0}C ± 5, 4 hrs
- Final samples E, F, and G were tested according to the highest iron reduction parameters from the 4M concentration.
    - Sample E – 1:2 S/L Ratio, 80 0C ± 5, 4 hrs
    - Sample F – 1:3 S/L Ratio, 80 0C ± 5, 4 hrs
    - Sample G - 1:4 S/L Ratio, 80 0C ± 5, 4 hrs

Anticipated observations were forecasted to show higher iron reduction compared to previous results, with this enhancement being attributed to the increased surface area facilitated by the presence of fine particles. Subsequent findings from diverse tests were detailed in Table 4.13.

Table 4.13: Summary: Results for Method 02

Sample	Initial Fe % (wt)	Final Fe % (wt)	Fe reduction % (wt)
Sample A	12.18	3.78	68.97
Sample B		3.48	71.43
Sample C		2.25	81.53
Sample D		2.11	82.68
Sample E		3.27	73.15
Sample F		2.03	83.33
Sample G		2.46	79.80

The results obtained from Method Two, using 90 µm passing samples, demonstrated over 80% iron reduction in samples C, D, and F compared to the initial sample. The highest iron reduction was observed in sample F, which was subjected to a 1:3 S/L ratio, 80°C ± 5°C, for 4 hours with a 4M concentration. When comparing samples F and G, despite sample G having a higher S/L ratio, it exhibited lower iron reduction than sample F. On average, the difference was considered negligible. However, it is noteworthy that all results achieving over 80% iron reduction involved 3M and 4M concentrations. This highlights the significant impact of concentration compared to other parameters, although the results were nearly identical for 3M and 4M concentrations.

These findings underscore the efficacy of concentration as a crucial factor in the iron reduction process. The results suggest that variations in concentration play a more substantial role in influencing iron reduction compared to alterations in the S/L ratio and temperature. Additionally, the data highlights the consistency of results between 3M and 4M concentrations, indicating that achieving over 80% iron reduction is feasible within this concentration range. Overall, the study concludes that concentration, particularly within the 3M to 4M range, is pivotal in optimizing the purification process, with particle size identified as the most influential parameter based on results from both methods.

Based on the results, the purification process is proven to be highly effective in achieving over 80% iron reduction by reducing particle size to less than 90 µm. A comprehensive analysis of results from both methods consistently highlights particle size as the most influential parameter in the purification process.

The findings emphasize that manipulating the particle size to this specific range significantly impacts the success of iron reduction. The ability to consistently achieve over 80% iron reduction underscores the reliability and effectiveness of this approach. Consequently, the study concludes that controlling particle size is a critical factor for optimizing the purification process. This insight offers valuable guidance for future applications and underscores the importance of understanding the role of particle size in achieving high-efficiency iron reduction during the purification process.

5. CONCLUSIONS

The separation of the raw materials to obtain minerals from beach sand in Pulmuddai, Sri Lanka was conducted by screening, spiral gravity separator, Wilfley table, and magnetic separation methods under wet and dry mediums, resulting in obtaining rutile with low iron content.

Then, the samples were analyzed by EDX to identify the mineral percentages and impurity contents. Initial samples showed 43.58% titanium and 16.91% iron content as impurities.

The purification of beach sand for titanium dioxide extraction has been successfully achieved through the leaching method utilizing hydrochloric acid. This process involves multiple parameters, with the particle size of the sand emerging as the most impactful factor for leaching and purification. The effectiveness of time and temperature mirrors that of acid concentration, with an optimal period of up to four hours, beyond which differences among samples become negligible.

Notably, the reduction of particle size to below 90µm, while maintaining specific process parameters (1:3 S/L Ratio, 80°C ± 5, 4 hrs, 4M concentration), results in an impressive 83.33% iron reduction after characterization of the purified samples. This underscores the critical role of particle size in achieving high-efficiency iron reduction during the leaching and purification process. The findings offer valuable insights for optimizing the purification process for titanium dioxide extraction, providing a clear roadmap for future applications in this field.

6. RECOMMENDATIONS

The following recommendations can be suggested based on the experiments conducted throughout the project.

1. Consider reducing the particle size further by grinding and ball milling techniques to achieve a higher percentage of iron reduction.
2. Explore the use of stronger acids and adjustments in pressure conditions to enhance iron reduction levels in the samples.

7. REFERENCES

[1] M. Nurdin, Maulidiyah, A. H. Watoni, N. Abdillah, and D. Wibowo, "Development of extraction method and characterization of TiO2 mineral from ilmenite," *Int. J. ChemTech Res.*, vol. 9, no. 4, pp. 483–491, 2016.

[2] V. J. Landis and J. H. Kaye, "Radiochemistry of Titanium," *Nucl. Sci. Ser.*, vol. 3034, p. 99, 1971.

[3] Z.-Y. Chen, K.-C. Chou, and F.-S. Li, "An Investigation of Electro-deoxidation Process for Producing Titanium from Dense Titanium Dioxide Cathode," *J. Manuf. Sci. Prod.*, vol. 13, no. 1–2, 2014.

[4] W. A. P. J. Premaratne and N. A. Rowson, "The processing of beach sand from Sri Lanka for the recovery of titanium using magnetic separation," *Phys. Sep. Sci. Eng.*, vol. 12, no. 1, pp. 13–22, 2003.

[5] L. H. Lalasari, R. Subagja, A. H. Yuwono, F. Firdiyono, S. Harjanto, and B. Suharno, "Sulfuric acid leaching of Bangka Indonesia ilmenite ore and ilmenite decomposed by NAOH," *Adv. Mater. Res.*, vol. 789, pp. 522–530, 2013.

[6] X. Hao, L. Lü, B. Liang, C. Li, P. Wu, and J. Wang, "Solvent extraction of titanium from the simulated ilmenite sulfuric acid leachate by trialkylphosphine oxide," *Hydrometallurgy*, vol. 113–114, pp. 185–191, 2012.

[7] T. H. Nguyen and M. S. Lee, "A Review on the Recovery of Titanium Dioxide from Ilmenite Ores by Direct Leaching Technologies," *Miner. Process. Extr. Metall. Rev.*, vol. 40, no. 4, pp. 231–247, 2019.

[8] R. Motsie and South Africa. Directorate: Mineral Economics, "An overview of South Africa's titanium mineral concentrate industry," p. 16, 2008.

[9] A. A. Zahir., "Green synthesis of silver and titanium dioxide nanoparticles using Euphorbia prostrata extract shows shift from apoptosis to G0/G1 arrest followed by necrotic cell death in Leishmania donovani," *Antimicrob. Agents Chemother.*, vol. 59, no. 8, pp. 4782–4799, 2015.

[10] K. Rasmussen., *Titanium Dioxide, NM-100, NM-101, NM-102, NM-103, NM-104, NM-105: Characterisation and Physico- Chemical Properties*. 2014.

[11] K. Mutombo, "Research and Development of Ti and Ti alloys: Past, present and future," *IOP Conf. Ser. Mater. Sci. Eng.*, vol. 430, no. 1, 2018.

[12] H. Bordbar, A. A. Yousefi, and H. Abedini, "titanium ores : A review," vol. 4, no. 2, 2017.

[13] Q. Wang, L. Jiang, F. Ni, and T. Wang, "The separation and concentration of titanium(IV) from sulfuric acid solution with trioctylamine," *Ind. Eng. Chem. Res.*, vol. 51, no. 8, pp. 3430–3435, 2012.

[14] Daniel Trujillo and Lucía Manangón, "Titanium Dioxide Recovery from Ilmenite Contained in Ferrotitaniferous Sands from Mompiche-Ecuador," *J. Geol. Resour. Eng.*, vol. 4, no. 4, pp. 175–183, 2016.

[15] A. J. Manhique and A. Sciences, "Titania Recovery from Low-grade Titaniferrous Minerals Philosophiae Doctor in Chemistry November 2012 Promoter : Professor Walter Focke," no. November, 2012.

[16] L. G. Mendoza-Reyes, E. R. de S. Miguel, J. P. Sánchez-Guerrero, D. Y. Pardo-Gaytán, and J. de Gyves, "Novel D2EHPA-polysiloxane-based sorbent for titanium (IV) extraction and separation," *J. Mex. Chem. Soc.*, vol. 55, no. 2, pp. 72–78, 2011.

[17] X. Xiong, Z. Wang, F. Wu, X. Li, and H. Guo, "Preparation of TiO2 from ilmenite using sulfuric acid decomposition of the titania residue combined with separation of Fe3+ with EDTA during hydrolysis," *Adv. Powder Technol.*, vol. 24, no. 1, pp. 60–67, 2013.

[18] J. Gambogi and S. J. Gerdemann, "Titanium Metal: Extraction to Application," *Rev. Extr. Process. Prop. Appl. React. Met.*, pp. 175–210, 2013.

[19] C. D. E. Alwis, "the Production of Liquid Titanium By Molten Oxide Electrolytic Production of," 2006.

[20] R. K. Singh and P. M. Dhadke, “Extraction and separation of titanium(IV) with D2EHPA and PC-88A from aqueous perchloric acid solutions,” *J. Serbian Chem. Soc.*, vol. 67, no. 7, pp. 507–521, 2002.

[21] A. C. Van Arkel, “History and Extractive Metallurgy,” *Titanium*, pp. 1–29, 2021.